

Research Article

Study on the Application Scheme of Aerodynamic Coefficient Identification Based on the Differential Evolution Algorithm

Pengfei Liu ¹, Hongsong Cao ¹, Shunshan Feng,² Hengzhu Liu ¹ and Ye Du ¹

¹College of Mechatronics Engineering, North University of China, Taiyuan 030051, China

²State Key Laboratory of Explosion Science and Technology, Beijing Institute of Technology, Beijing 100081, China

Correspondence should be addressed to Hongsong Cao; chs@nuc.edu.cn

Received 22 April 2020; Accepted 25 June 2020; Published 5 August 2020

Academic Editor: Francesca Vipiana

Copyright © 2020 Pengfei Liu et al. This is an open access article distributed under the Creative Commons Attribution License, which permits unrestricted use, distribution, and reproduction in any medium, provided the original work is properly cited.

The present paper studies the application schemes of aerodynamic coefficient identification based on the differential evolution (DE) algorithm from free flight data. Two identification schemes utilizing the DE algorithm are proposed, including the whole discrete point (WDP) scheme and the differential interval linear (DIL) scheme. Several comparative tests are conducted to study the performances of the two schemes by using the noisy simulated flight data and the measured radar data. The results show satisfactory performance in estimating the aerodynamic coefficients for the two schemes. The WDP scheme provides more accurate and robust coefficients estimates in exchange of more than two times greater computational effort compared with the DIL scheme.

1. Introduction

The identification of aerodynamic coefficients, based on free flight data, is one of the important technologies in the field of projectile aerodynamics [1–5]. Compared with wind tunnel tests or numerical methods, aerodynamic coefficient identification can use actual flight data and full-scale projectiles. This could ensure higher fidelity and enable it to become a critical approach for determining the aerodynamic coefficients, especially in the verification phase of aerodynamic configuration design, ballistic flight control design, and fire table generation [1, 2, 6–11].

In recent years, with the improvements in computer performance, modern intelligence optimization algorithms have been developed and applied to identify aerodynamic coefficients. Compared with the traditional gradient-based identification method [12–21], intelligence optimization algorithms have extreme superiority in obtaining the global optimum and handling discontinuous nonconvex objectives [22]. Due to the great value in academics and engineering, a lot of work has been devoted to the research of intelligence optimization algorithms for aerodynamic coefficient identification. The genetic algorithm (GA) was used to estimate

projectile aerodynamic coefficients from free flight range data [21]. The adaptive GA was used for nonlinear aerodynamic parameter identification of an axis-symmetrical tactical missile [23]. The partial swarm optimization (PSO) algorithm was applied to the aerodynamic coefficient identification of a spinning symmetric projectile [24]. The artificial bee colony (ABC) algorithm was applied to identify the high angle of attack aerodynamic parameters [25].

The differential evolution (DE) algorithm proposed by Storn and Price is a differential operator-based evolutionary optimization technique [26–28]. This algorithm requires very few control parameters and adopts real number coding to add diversity to the difference distributions [27–29]. These unique features make it accurate, robust, easy to use, and converge fast compared with previous intelligence optimization algorithms. The DE algorithm has already been successfully used in the fields of aerodynamic design, mechanical design, and digital filter design [26, 30–32].

In the aerodynamic coefficient identification from the whole trajectory data, it is well known that a key process is to split the measurements into multiple small intervals, and then, the coefficients can be identified in the intervals. In the previous research [1, 2, 12, 13, 15–19, 21, 23–25], the coefficients in an

interval are usually modeled as constants. In the work of Zaikang and Lyster, the drag coefficients in each interval are modeled as a cubic spline [17]. The identification results are in good agreement with the measured data. However, due to the limited measurements of the small interval and the constant assumption of the coefficient, the unbalanced noise distribution would lead to overfitting of the data, and the coupling effect between the data intervals would be ignored. These drawbacks reduced the accuracy and robustness.

In this article, two identification schemes based on the DE algorithm are proposed to improve the performance of identifying the aerodynamic coefficients from trajectory data, including the whole discrete point (WDP) scheme and the differential interval linear (DIL) scheme. Several comparative tests are conducted, and the characteristics of these two schemes with regard to the computational time, accuracy, and robustness are discussed.

2. Projectile Flight Dynamic Model

In this study, the system model of aerodynamic coefficient identification is a standard six-degree-of-freedom (6-DOF) model typically used in flight dynamic modeling of projectiles. Figure 1 gives two standard reference frames used to develop this model. The 6-DOF model consists of the inertial position components of the projectile mass center (x, y, z) from an inertial frame and the standard aerospace sequence Euler angles (γ, ϕ_2, ϕ_a).

The kinematic and dynamic differential equations for describing the motion of the projectile in flight are given as follows [1, 33]:

$$\begin{bmatrix} \dot{x} \\ \dot{y} \\ \dot{z} \end{bmatrix} = \begin{bmatrix} \cos \phi_2 \cos \phi_a & -\sin \phi_a & -\sin \phi_2 \cos \phi_a \\ \cos \phi_2 \sin \phi_a & \cos \phi_a & -\sin \phi_2 \sin \phi_a \\ \sin \phi_2 & 0 & \cos \phi_2 \end{bmatrix} \begin{bmatrix} u \\ v \\ w \end{bmatrix}, \quad (1)$$

$$\begin{bmatrix} \dot{\gamma} \\ \dot{\phi}_2 \\ \dot{\phi}_a \end{bmatrix} = \begin{bmatrix} 1 & 0 & -\tan \phi_2 \\ 0 & -1 & 0 \\ 0 & 0 & \frac{1}{\cos \phi_2} \end{bmatrix} \begin{bmatrix} p \\ q \\ r \end{bmatrix}, \quad (2)$$

$$\begin{bmatrix} \dot{u} \\ \dot{v} \\ \dot{w} \end{bmatrix} = \begin{bmatrix} \frac{X}{m} \\ \frac{Y}{m} \\ \frac{Z}{m} \end{bmatrix} + \begin{bmatrix} 0 & -r & q \\ r & 0 & -r \tan \phi_2 \\ -q & r \tan \phi_2 & 0 \end{bmatrix} \begin{bmatrix} u \\ v \\ w \end{bmatrix}, \quad (3)$$

$$\begin{bmatrix} \dot{p} \\ \dot{q} \\ \dot{r} \end{bmatrix} = \begin{bmatrix} I_A & 0 & 0 \\ 0 & I_C & 0 \\ 0 & 0 & I_C \end{bmatrix}^{-1} \begin{bmatrix} L \\ M \\ N \end{bmatrix} + \begin{bmatrix} 0 & -r & q \\ r & 0 & -r \tan \phi_2 \\ -q & r \tan \phi_2 & 0 \end{bmatrix} \begin{bmatrix} I_A p \\ I_C q \\ I_C r \end{bmatrix}. \quad (4)$$

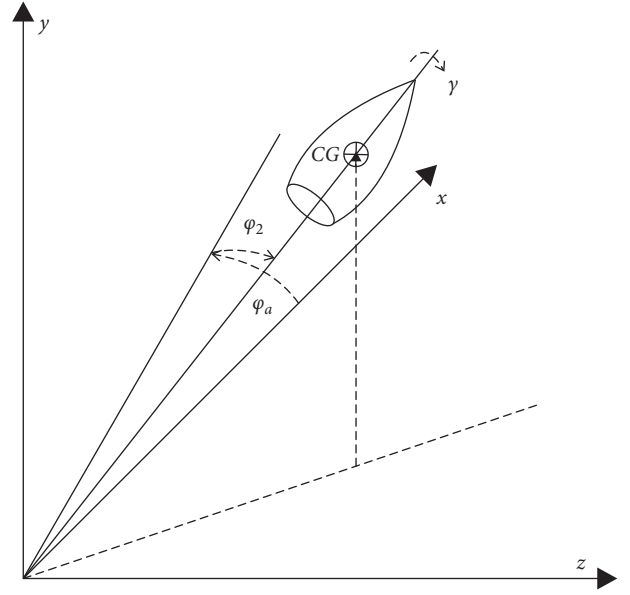


FIGURE 1: Schematic of the projectile's position coordinates.

The forces acting on the projectile in (3) consist of gravity (G) and the aerodynamic force. The aerodynamic force is split into a standard aerodynamic force (A) and Magnus aerodynamic force (M). Gliding flight is assumed in this study. The combination of forces is expressed in the following equation:

$$\begin{bmatrix} X \\ Y \\ Z \end{bmatrix} = \begin{bmatrix} X_G \\ Y_G \\ Z_G \end{bmatrix} + \begin{bmatrix} X_A \\ Y_A \\ Z_A \end{bmatrix} + \begin{bmatrix} X_M \\ Y_M \\ Z_M \end{bmatrix}, \quad (5)$$

$$\begin{bmatrix} X_G \\ Y_G \\ Z_G \end{bmatrix} = -mg \begin{bmatrix} \cos \phi_2 \sin \phi_a \\ \cos \phi_a \\ -\sin \phi_2 \sin \phi_a \end{bmatrix}, \quad (6)$$

$$\begin{bmatrix} X_A \\ Y_A \\ Z_A \end{bmatrix} = \frac{1}{2} \rho V_{CG}^2 S \left(-C_D \begin{bmatrix} -\cos \alpha \cos \beta \\ \sin \alpha \\ \cos \alpha \cos \beta \end{bmatrix} + C_{l\alpha} \begin{bmatrix} \sin^2 \beta + \cos^2 \beta \sin^2 \alpha \\ -\sin \beta \cos \alpha \cos \beta \\ -\cos^2 \beta \sin \alpha \cos \alpha \end{bmatrix} \right), \quad (7)$$

$$\begin{bmatrix} X_M \\ Y_M \\ Z_M \end{bmatrix} = \frac{1}{2} \rho V_{CG}^2 S C_{y_{pa}} \left(\frac{p d}{V_{CG}} \right) \begin{bmatrix} 0 \\ -\sin \alpha \cos \beta \\ \sin \beta \end{bmatrix}. \quad (8)$$

In (7), the drag coefficient C_D is estimated by considering the zero-yaw drag coefficient C_{D0} and the yaw drag coefficient C_{D2} [2]:

$$C_D = C_{D0} + C_{D2} = C_{D0} + (C_{l\alpha} + 0.5C_{D0})(\alpha^2 + \beta^2). \quad (9)$$

It is known that C_D has the most significant effect on the trajectory, and C_{D0} represents the main part of C_D [34].

The moment acting on the projectile in (4) consists of the moment due to A , the moment due to M , and the unsteady aerodynamic moments (UA), as shown in the following equation:

$$\begin{bmatrix} L \\ M \\ N \end{bmatrix} = \begin{bmatrix} L_A \\ M_A \\ N_A \end{bmatrix} + \begin{bmatrix} L_M \\ M_M \\ N_M \end{bmatrix} + \begin{bmatrix} L_{UA} \\ M_{UA} \\ N_{UA} \end{bmatrix}. \quad (10)$$

The moments in (10) are expressed as follows:

$$\begin{bmatrix} L_A \\ M_A \\ N_A \end{bmatrix} = \frac{1}{2} \rho S V_{CG}^2 C_{m\alpha} \begin{bmatrix} 0 \\ \sin \alpha \cos \beta \\ -\sin \beta \end{bmatrix}, \quad (11)$$

$$\begin{bmatrix} L_M \\ M_M \\ N_M \end{bmatrix} = \frac{1}{2} \rho S V_{CG}^2 (-C_{np\alpha}) \left(\frac{pd}{V_{CG}} \right) \begin{bmatrix} 0 \\ -\sin \beta \\ -\sin \alpha \cos \beta \end{bmatrix}, \quad (12)$$

$$\begin{bmatrix} L_{UA} \\ M_{UA} \\ N_{UA} \end{bmatrix} = \frac{1}{2} \rho S V_{CG}^2 \begin{bmatrix} C_{lDD} + C_{lp} \frac{pd}{V_{CG}} \\ C_{mq} \frac{qd}{V_{CG}} \\ C_{mq} \frac{rd}{V_{CG}} \end{bmatrix}. \quad (13)$$

The aerodynamic angles of attack α and β are then defined by the following:

$$\tan \alpha = \frac{w}{u}, \quad (14)$$

$$\tan \beta = \frac{v}{\sqrt{u^2 + w^2}}. \quad (15)$$

The above equations are the major equations of the projectile flight dynamic model. More details regarding the projectile flight model can be found in [33]. All aerodynamic coefficients (C_{D0} , C_{D2} , $C_{l\alpha}$, $C_{yp\alpha}$, $C_{m\alpha}$, $C_{np\alpha}$, C_{lDD} , C_{lp} , and C_{mq}) depend upon the local Mach number and are obtained during simulation by linear interpolation. To solve this model, the fourth-order Runge–Kutta algorithm is employed in this article. In addition, all calculations are performed with a real record of meteorological data.

3. DE Algorithm-Based Aerodynamic Coefficient Identification

As mentioned above, the aerodynamic coefficient identification problem can be posed as an optimization problem; the basic task is to seek the set of coefficients (θ) that best fit the measured data, namely, to minimize the cost function $O(\theta)$ at different Mach numbers. In this article, the

maximum likelihood criterion is chosen to formulate the object cost function, and thus, $O(\theta)$ is defined as follows:

$$O(\theta) = \sum_{i=1}^n [\varepsilon^T(i) R^{-1} \varepsilon(i) + \ln|R|], \quad (16)$$

where θ is the vector of unknown coefficients and $\varepsilon(i)$ is the deviation of the measured state vector from the calculated state vector, which is defined as follows:

$$\varepsilon(i) = \mathbf{H}_M - \mathbf{H}_C, \quad (17)$$

where \mathbf{H}_M and \mathbf{H}_C are the measured and calculated state vectors, respectively, which are obtained from the 6-DOF dynamic simulation with the identified coefficients in one step. R is the covariance matrix of measurement noise. As the statistical property of the measurement noise is unknown, the optimum estimation \hat{R} usually replaces R :

$$R \approx \hat{R} = \frac{1}{n} \sum_{i=1}^n \varepsilon(i) \varepsilon^T(i). \quad (18)$$

The detailed implementation steps for the identification of aerodynamic coefficients using the DE algorithm can be described as follows.

Step 1 (initialization operation): generate NP ($i = 1 \dots NP$) individuals randomly in the whole search space. The initial population is given by the following:

$$\theta_k^{i,G} = \theta_L^{i,G} + r \times (\theta_U^{i,G} - \theta_L^{i,G}), \quad (19)$$

where r is a uniformly distributed random number in the interval $[0, 1]$ and $\theta_k^{i,G}$ is the k^{th} component of the individual θ^i in the G generation. $\theta_L^{i,G}$ and $\theta_U^{i,G}$ are the lower and upper bounds of $\theta_k^{i,G}$, respectively.

Step 2: evaluate the fitness of each individual in the population according to (16).

Step 3: create a new population as follows:

(a) **Mutation operation:** a mutant vector is generated according to the following:

$$V_k^{i,G} = \theta_k^{r1,G} + F(\theta_k^{r2,G} - \theta_k^{r3,G}). \quad (20)$$

(b) **Crossover operation:** a new trail vector is generated by mixing the mutant vector and the target vector.

$$U_k^{i,G} = \begin{cases} V_k^{i,G}, & \text{if } r^k \leq CR^{i,G} \text{ or } k = k_{\text{rand}}, \\ \theta_k^{i,G}, & \text{otherwise,} \end{cases} \quad (21)$$

where r^k is a random number taken from the uniform distribution $[0, 1]$.

(c) **Selection operation:** selection determines whether the target or the trial vector survives to the next iteration. For each mutant vector and its corresponding target vector in the current population,

the object function values are compared using a greedy selection scheme. The selection operation is described as follows:

$$\theta_k^{i,G} = \begin{cases} U_k^{i,G+1}, & \text{if } O(U_k^{i,G+1}) < O(U_k^{i,G}), \\ \theta_k^{i,G}, & \text{otherwise.} \end{cases} \quad (22)$$

Step 4: repeat steps 2-3 until the termination criteria are satisfied. In this article, the termination criteria are defined as follows:

$$G > G_{\max}. \quad (23)$$

The flowchart of the implemented DE algorithm is shown in Figure 2.

4. Identification Schemes

The first scheme, which is the whole discrete point (WDP) scheme, as shown in Figure 3, treats the measured trajectory as a whole. The trajectory would not be divided into several intervals, and all of the coefficients corresponding to different Mach numbers in an aerodynamic coefficients table would be identified simultaneously. In this scheme, the design variable is defined as follows:

$$\theta = [C_{M_1}, C_{M_2}, \dots, C_{M_j}, \dots, C_{M_{j-1}}, C_{M_j}]^T, \quad (24)$$

where C_{M_j} represents the coefficient corresponding to the j th Mach number in the coefficients table, $j = 1, 2, \dots, J$, and J is the number of Mach numbers. The dimension of an individual in population k is equal to the number of Mach numbers J .

In the second scheme, which is the differential interval linear (DIL) scheme, as shown in Figure 3, the whole trajectory would be divided into several intervals. The relationship between the coefficients and the Mach numbers in an interval is treated as a linear function, where the slope does not have to be zero. A constant factor K_{M_n} in each interval is introduced in this scheme, which is defined as follows:

$$K_{M_n} = \frac{C_{\text{real}}}{C_{\text{prior}}}. \quad (25)$$

As seen from (25), K_{M_n} represents the gap between the prior value and the real value of aerodynamic coefficients, and C_{real} can be determined by identifying K_{M_n} in each interval successively from the free flight data. Namely, K_{M_n} becomes the design variable in this optimization problem, which is defined as follows:

$$\theta = K_{M_n}, \quad (26)$$

where $n = 1, 2, \dots, N$, and N is the number of intervals. It is easy to find that the dimension of an individual in population k in this scheme is equal to the number of the correction factors in each interval.

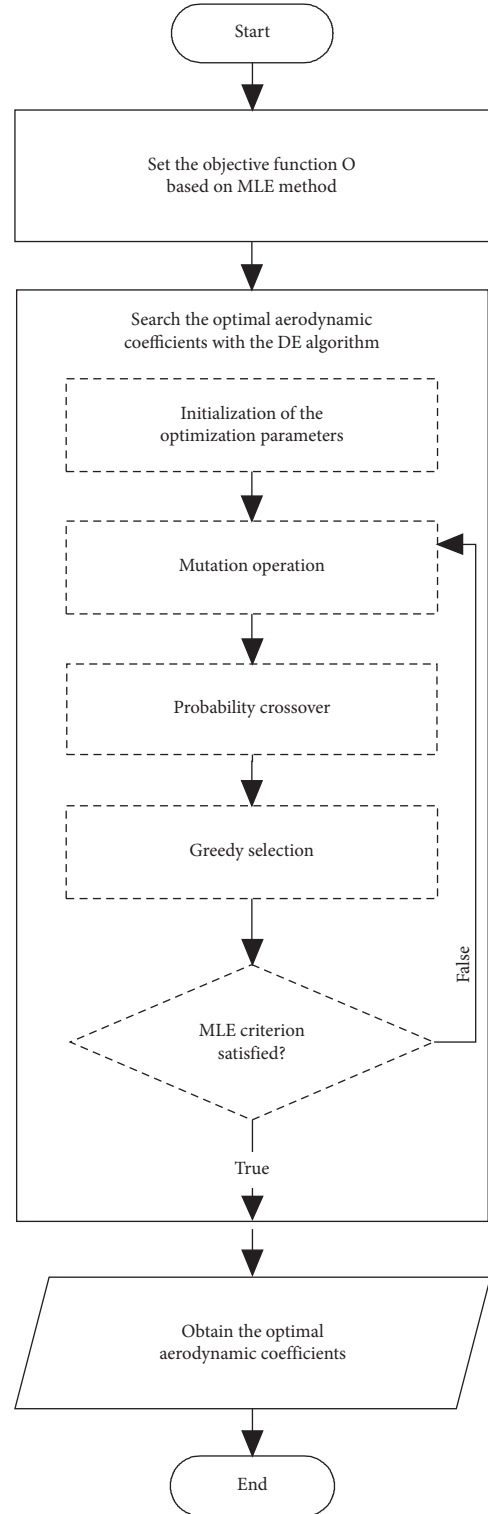


FIGURE 2: Flowchart of the implemented DE algorithm.

In addition, for comparison research, the conventional differential interval constant (DIC) scheme is used in this paper. This scheme divides the whole trajectory into several intervals as in the DIL scheme; yet, the coefficients in each interval are modeled as constants and identified successively. In this scheme, the design variable is defined as follows:

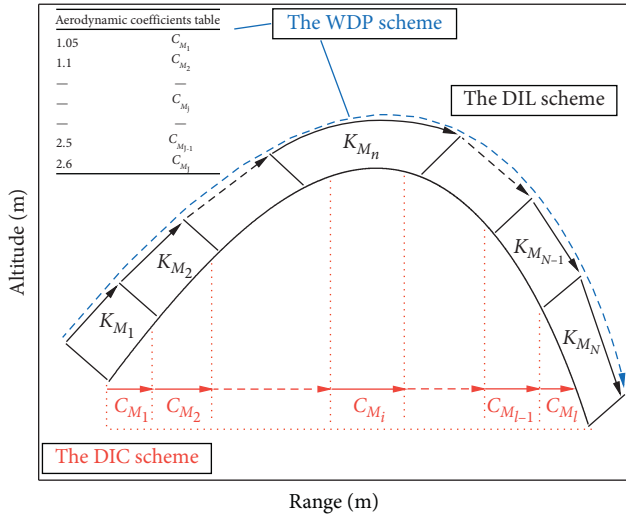


FIGURE 3: Schematic diagram of the identification schemes.

$$\theta = C_{M_i}, \quad (27)$$

where C_{M_i} represents the coefficient in the i th interval, $i = 1, 2, \dots, I$, and I is the number of intervals. The dimension of an individual in population k in this scheme is equal to the number of coefficients in each interval.

Additionally, the prior information, namely, the general trend or characteristics, is required for all of the schemes mentioned above. This prior information could be used to divide the Mach number interval, to set lower and upper bounds of the design variable, to obtain the feasibility of identification, etc. In practical engineering, the prior information could be obtained from wind tunnel tests, numerical methods, or engineering experience.

5. Results and Discussion

Several comparative tests are conducted in two different scenarios to study the performances of the identification schemes presented in this paper. A fin-stabilized projectile is selected as the test bed, and the physical characteristics of this projectile are listed in Table 1. In order to simplify the problem, the present study focuses on the identification of the drag coefficient, and the methods presented in this paper could be easily used for other aerodynamic coefficients. Other aerodynamic coefficients are input as known values.

In the first scenario, the simulated measurement data is generated from a 6-DOF projectile dynamic simulation. To model the random noise, which inevitably exists in the trajectory data measured by radar, the Gaussian noise is added into the simulated position and velocity. Three standard deviations are used equal to 0.2, 1.0, and 5.0 times the nominal standard deviation are considered, and the nominal standard deviation σ is 3 m and 0.01 m/s for the position and velocity, respectively. The identification is conducted 50 times for each scheme, and the final identification results are the average values of the 50 identification results. The meteorological data and the initial launch conditions used in this scenario are chosen to be the same as

the second scenario, which will be described in the next paragraph.

In the second scenario, phased array radar data from a free flight test is used as the measurement data to identify the aerodynamic drag coefficient. In this test, available measurements are the position data and radial velocity data, and the meteorological data were recorded with both ground and balloon-carried instruments throughout the test events. In Figure 4, the recorded data for the pressure, temperature, wind speed, and wind direction as a function of the altitude are shown. For the present projectile, the meteorological data below 12 km is mainly used. In Table 2, the initial launch conditions of the test are listed.

Table 3 describes the initialization of the parameters implemented in the DE algorithm. The main control parameters that need to be set are the number of individuals (NP), the weight factor (F), and the crossover rate (CR). Every control parameter is tuned through appropriate tradeoff studies for the optimal process. Detailed information about the principle of tuning the control parameters can be found in [27, 28, 30, 35]. In addition, to improve the efficiency of identification processing, the multiprocessing technique is used in the program.

In Figure 5, the reconstructions of the trajectory with the identification results from two scenarios are plotted, including the altitude versus range and radial velocity versus range. In the first scenario (Figures 5(a)–5(c)), as can be observed, the match error enlarged with the increase of the noise. In Figure 5(c), relatively significant error can be found, especially in the apex of the trajectory. There is a possibility of high sensitivity of the drag coefficient in the transonic region. In Figure 5(d), in the descent stage of the trajectory, the error appears to be enlarged. It is possible that due to the limit of the performance of the radar system, the noise existing in the measured radar trajectory data enlarged with the increase of the range, which reduced the accuracy of identification at the descent stage.

In Figure 6, the identification results from the first scenario at varying levels of noise are plotted. It is used for closer inspection of the performance of the identification schemes introduced in the present paper. It can be seen that the WDP scheme gives the most accurate result. This is consistent with the results presented in Figure 5. As can be observed from Figure 5, the reconstruction of the trajectory of the WDP schemes matches the true data very well whether in the apex region or the descent stage of the two scenarios. This is because more measurements are considered in the WDP scheme, which enable the sampled noise to approach a normal distribution, and then leads to a more consistent nominal cost. This advantage can avoid the overfitting of data and increase the accuracy of the identification. Additionally, because the WDP scheme identifies all of the coefficients at different Mach numbers simultaneously, the error generated in the early stage of the trajectory would not be accumulated and spread to the later stage. In contrast, since the DIC scheme and the DIL scheme identified the coefficients along the trajectory interval successively, the coupling error would gradually accumulate and reduce the identification accuracy. Additionally, in each interval of the

TABLE 1: The projectile's physical properties.

m (kg)	I_A (kg-m ²)	I_C (kg-m ²)	CG from nose (m)	d (m)
45.340	0.115	31.627	1.190	0.122

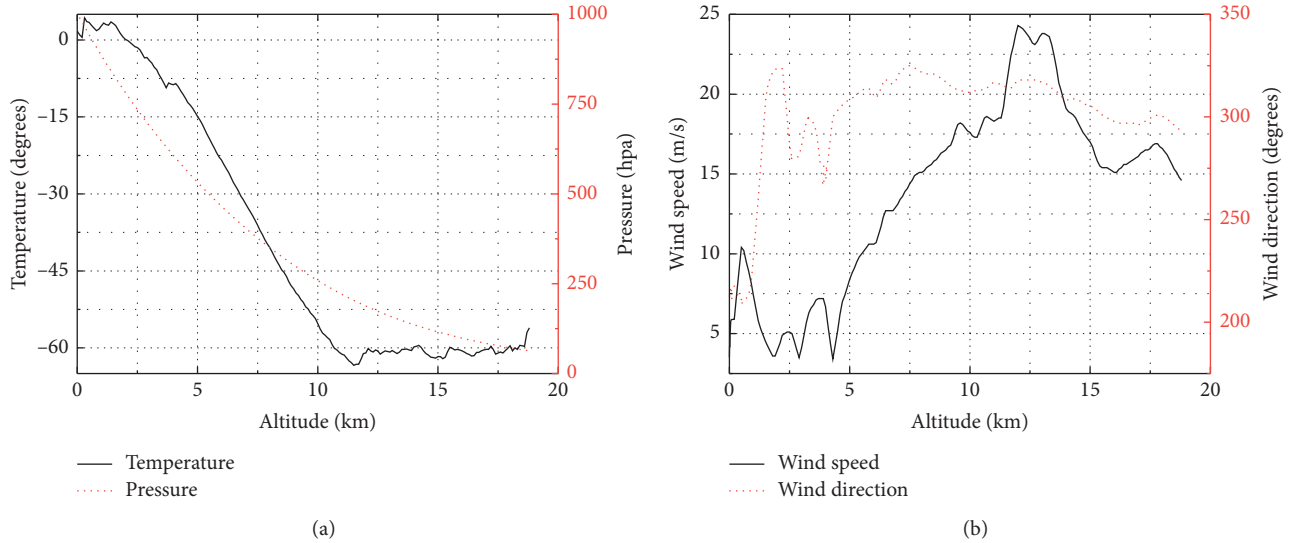


FIGURE 4: Meteorological data versus altitude. (a) Temperature and pressure versus altitude. (b) Wind speed and wind direction versus altitude.

TABLE 2: Initial conditions for the two scenarios.

State	First scenario/second scenario
Launching elevation angle (degrees)	42.7
Launching azimuth angle (degrees)	358.953
Velocity (m/s)	41.317
Spin rate (rad/s)	25.133

TABLE 3: Parameter initialization for the three schemes.

Parameters	Identification schemes		
	DIL	WDP	DIC
Number of individuals (NP)	80	160	80
Weight factor (F)		0.8	
Crossover rate (CR)		0.9	
Maximum number of generations (G_{max})		300	
Mutation strategy		DE/current-to-best/1/bin	
Selection strategy		Best-parent-child	
Termination criteria		G_{max}	
Number of measurement data in interval	25	All	25
Number of parallel processes		15	

aerodynamic coefficients table, the coefficients are obtained by linear interpolation. It is actually that the coefficients are treated as linear function of Mach number, and the WDP scheme identifies both the slope and intercept. Namely, the

WDP scheme can use the first-order information of the model of aerodynamic coefficients.

For the DIL scheme, it is intended to improve the identification accuracy. However, as can be observed from Figures 5 and 6, the accuracy of the DIL scheme is much closer to that of the conventional DIC scheme. It is found that the sums of the absolute error of the range from the second scenario for the DIL scheme and the DIC scheme are $1.5E+5$ and $2.15E+5$, respectively, whereas it is $3.1E+4$ for the WDP scheme. It is possible that the prior information is not accurate enough. Although the DIL scheme models the coefficients in an interval with a linear function instead of a constant function as in the DIC scheme, the specific form of the linear function, namely, the prior information, may not be close enough to the real value. Moreover, the introduced correction factor would simultaneously affect the slope and intercept, which would lose some accuracy. In the future work, it is suggested to choose both the slope and intercept as design variables to be identified in the WDP scheme. Moreover, in Figure 6(c), significant fluctuation from the results of the DIC scheme can be observed, especially in the transonic region. This is because the DIC scheme uses constants to model the aerodynamic coefficients, which means that the converging order is zero order. In the field of optimization, it also means that the robustness of the DIC scheme is worse than that of the WDP scheme and the DIL scheme.

In Figure 7, the computation CPU times using different schemes with simulated data and radar data are plotted. In all of the tests, the computation CPU times for the DIC

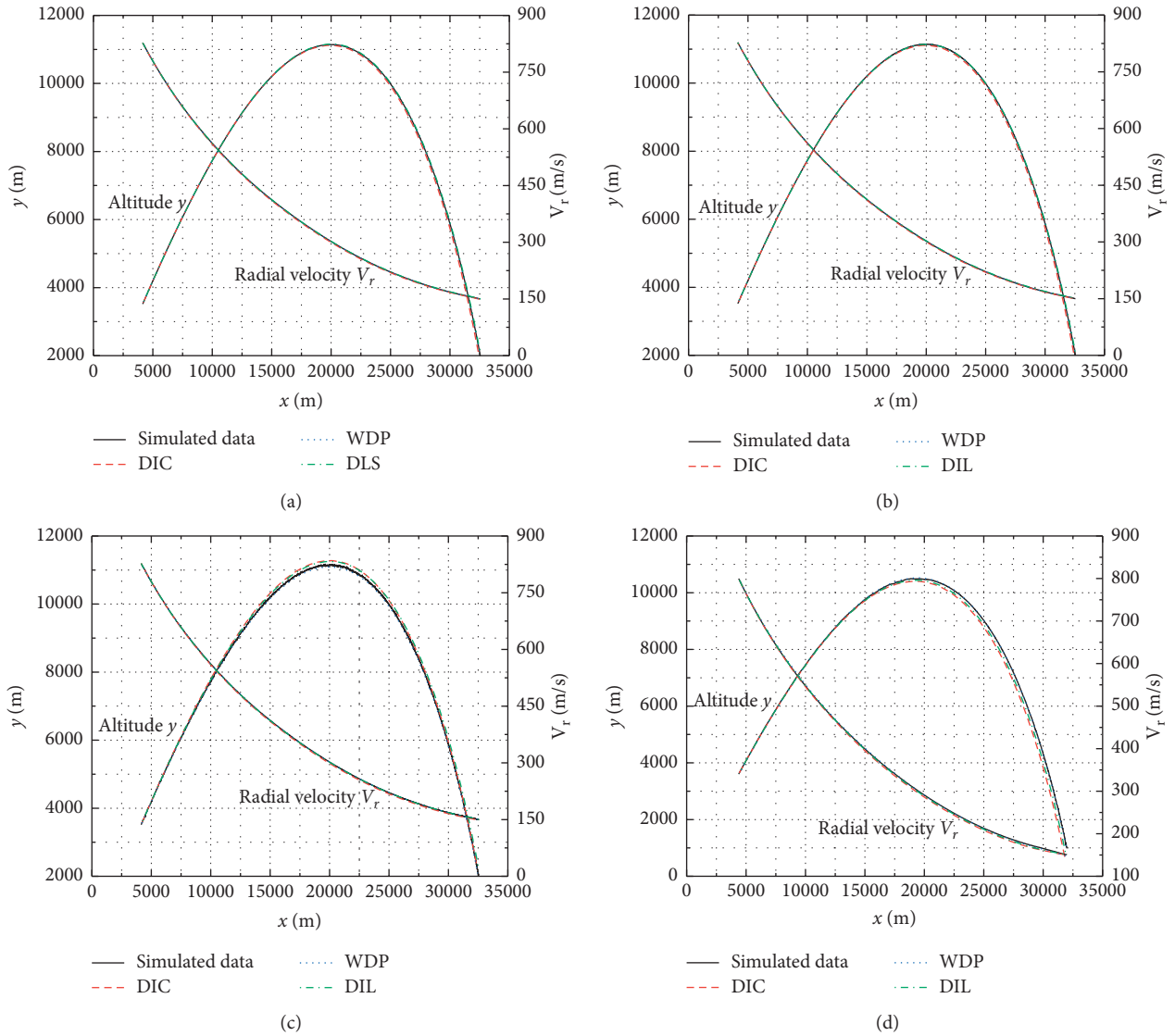


FIGURE 5: The trajectory matching for different schemes from the two scenarios. (a) $\sigma_{noise} = 0.2\sigma$. (b) $\sigma_{noise} = 1.0\sigma$. (c) $\sigma_{noise} = 5.0\sigma$. (d) Radar data.

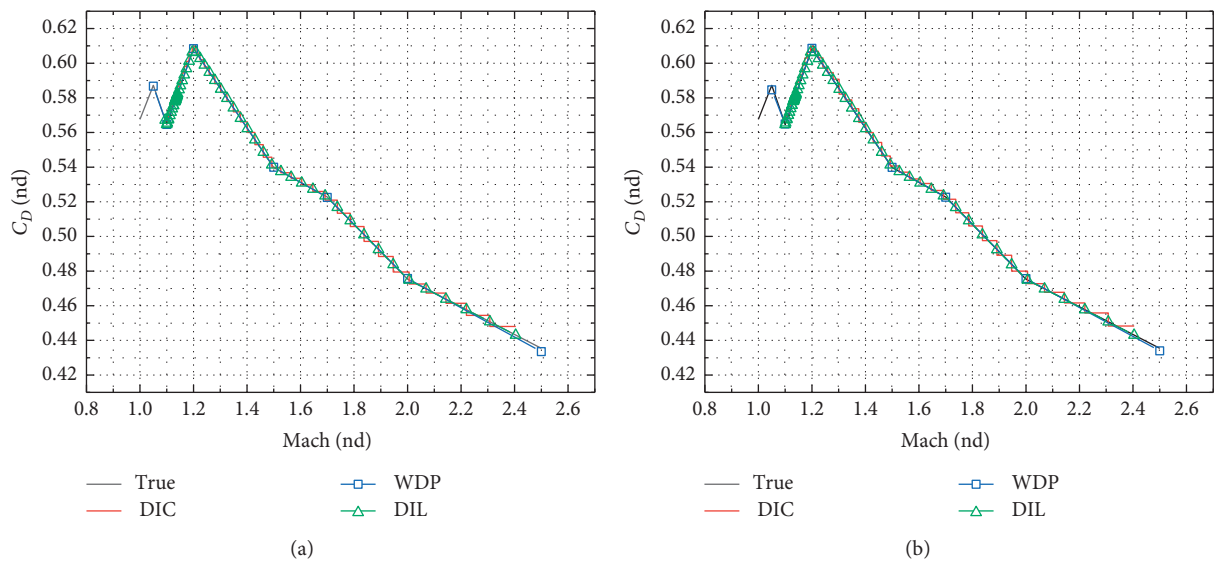


FIGURE 6: Continued.

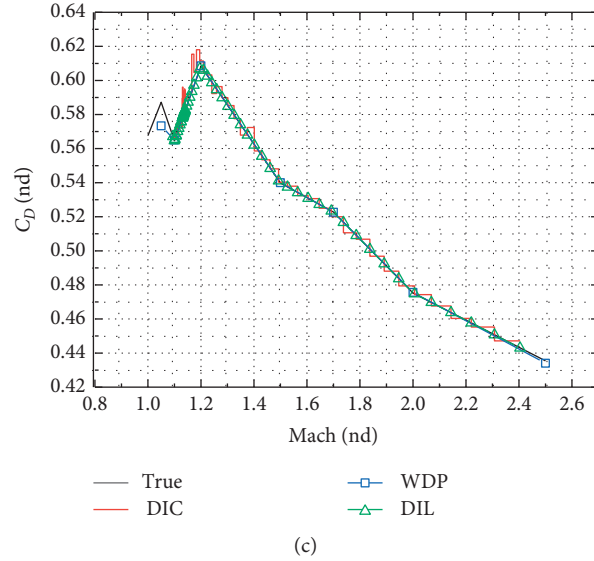


FIGURE 6: Identification results from simulated radar data for three schemes. (a) $\sigma_{noise} = 0.2\sigma$. (b) $\sigma_{noise} = 1.0\sigma$. (c) $\sigma_{noise} = 5.0\sigma$.

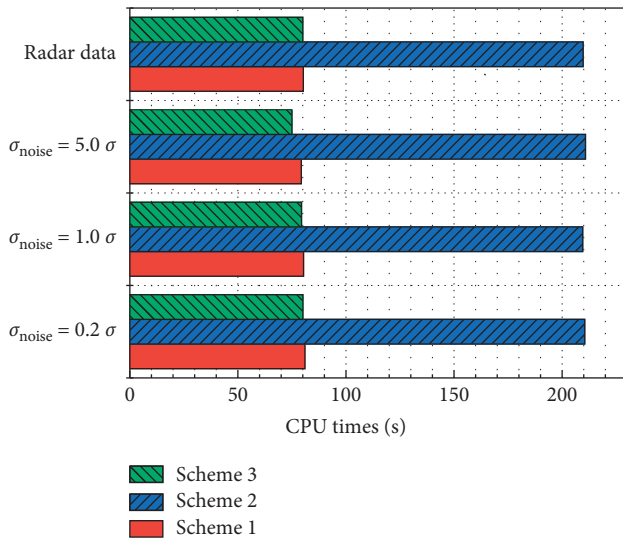


FIGURE 7: Mean computation CPU times.

scheme and the DIL scheme are very close to each other, which varied from 75 s to 81 s. For the WDP scheme, the computation time is much longer than that of the other two schemes. As seen from Figure 7, the computation CPU time for the WDP scheme is up to 211 s.

A direct reason for this situation is that the WDP scheme has larger computational budgets in each iteration of the optimization process since the dimension of an individual in the population is much higher than that in the DIC scheme and the DIL scheme. In the present study, we choose the drag coefficient as the identified parameter. According to (24), (26), and (27), the dimension of the identification problem for the DIC scheme and the DIL scheme is one, and the dimension for the WDP scheme depends upon the number of Mach numbers in the aerodynamic coefficients table. In the present study, the number of Mach numbers is 9.

Although the WDP scheme has advantages with regard to accuracy and robustness compared with the other two schemes, it is in exchange of greater computational effort. However, with the development of computer science and technology, an acceptable level of the computational time could be achieved by utilizing high-performance computing technology, such as the parallel computation used in the present paper. Additionally, one can improve the efficiency of the identification by using multiple schemes. For example, in the different Mach number regions, one can apply the different schemes depending upon the degree of fluctuation of the aerodynamic coefficients. For the WDP scheme, one can divide the trajectory into two or three intervals to improve the efficiency while maintaining the accuracy in cases, where the number of Mach numbers in the aerodynamic coefficients table is much more than 9, as in the present paper.

6. Conclusions

Two identification schemes based on DE algorithm-based aerodynamic coefficient identification are proposed. Several comparative tests are conducted by identifying the aerodynamic coefficients from the noisy simulated flight data and radar data. The results show that both schemes presented in this paper can accurately estimate the aerodynamic coefficients. The WDP scheme and the DIL scheme improve the robustness of the identification based on the DE algorithm. Since the WDP scheme treats the trajectory as a whole, which effectively reduces the coupling error, the WDP scheme gives relatively better identification results compared with the DIL scheme and the DIC scheme. However, the computation times are more than two times greater compared with the other two schemes.

For application of the DE algorithm-based projectile aerodynamic coefficient identification in practical engineering, it is suggested that future work should focus on the following

objectives. First, the fusion of multiple schemes or a new scheme might be developed to improve the overall identification performance with limited measurements. Second, the efficiency of the DE algorithm should be further improved, especially in dealing with multidimensional problems.

Nomenclature

Projectile Dynamic Model

(I_A, I_C, I_C) :	Projectile inertia components ($\text{kg} \cdot \text{m}^2$)
(p, q, r) :	Projectile angular velocity vector components (rad/s)
(u, v, w) :	Projectile linear velocity vector components (m/s)
(x, y, z) :	Projectile location vector components (m)
(α, β) :	Projectile aerodynamic angles of attack (rad)
$(\gamma, \varphi_2, \varphi_a)$:	Projectile Euler angles (rad)
(X, Y, Z) :	Aerodynamic force vector components (N)
(L, M, N) :	Aerodynamic moment vector components ($\text{N} \cdot \text{m}$)
ρ :	Atmospheric density (kg/m^3)
d :	Projectile reference diameter (m)
l :	Projectile reference length (m)
S :	Projectile reference area (m^2)
CG :	Projectile center of gravity location from the nose (m)
m :	Projectile mass (kg)
V_{CG} :	Magnitude of the mass center velocity (m/s)
V_r :	Projectile radial velocity (m/s)
C_D :	Drag coefficient
C_{D0} :	Zero-yaw drag coefficient
C_{D2} :	Yaw drag coefficient ($1/\text{rad}^2$)
C_{Ia} :	Lift force coefficient derivative with respect to the total yaw angle ($1/\text{rad}$)
C_{ypa} :	Magnus force aerodynamic coefficient ($1/\text{rad}^2$)
C_{ma} :	Pitching moment aerodynamic coefficient ($1/\text{rad}$)
C_{npa} :	Magnus moment aerodynamic coefficient ($1/\text{rad}^2$)
C_{lDD} :	Roll moment aerodynamic coefficient due to fin cant ($1/\text{rad}$)
C_{lp} :	Roll rate damping moment aerodynamic coefficient ($1/\text{rad}$)
C_{mq} :	Pitch rate damping moment aerodynamic coefficient ($1/\text{rad}$)

Differential Evolution

H :	State vector of the ballistic model
ε :	Deviations of the measured state from the calculated state
O :	Object function
n :	Number of the measured points
Ma :	Mach number
$[Ma_1, Ma_2]$:	Mach number interval
$DE/md/c$:	m , vector to be perturbed; d , number of difference vectors; c , type of crossover

NP :	Number of individuals
G :	Number of generations
k, k_{max} :	Parameters within the vectors
V :	Mutant vector
U :	Target vector
F :	Weight factor
CR :	Crossover rate.

Subscripts

E :	Earth frame
D :	Aerodynamic drag force vector components
C, M :	Calculated and measured states of the projectile
L, U :	Lower and upper limits of the search space.

Data Availability

The data used to support the findings of this study are available from the corresponding author upon request.

Conflicts of Interest

The authors declare that there are no conflicts of interest regarding the publication of this paper.

Acknowledgments

This research was supported by the Natural Science Foundation of North University of China (Grant no. XJJ201806).

References

- [1] R. L. McCoy, *Modern Exterior Ballistics: The Launch and Flight Dynamics of Symmetric Projectiles*, Schiffer Pub, Atglen, PA, USA, 2nd edition, 2012.
- [2] H. Zipeng, *Exterior Ballistics of Projectile and Rockets*, Beijing Institute of Technology Press, Beijing, China, 2008.
- [3] K. W. Iliff, "Parameter estimation for flight vehicles," *Journal of Guidance, Control, and Dynamics*, vol. 12, no. 5, pp. 609–622, 1989.
- [4] V. Klein and E. A. Morelli, *Aircraft System Identification: Theory and Practice*, American Institute of Aeronautics and Astronautics, Reston, VA, USA, 2006.
- [5] R. V. Jategaonkar, *Flight Vehicle System Identification: A Time Domain Methodology*, American Institute of Aeronautics and Astronautics, Reston, VA, USA, 2006.
- [6] P. Wernert and S. Theodoulis, "Modelling and stability analysis for a class of 155 mm spin-stabilized projectiles with course correction fuse (CCF)," in *Proceedings of the AIAA Atmospheric Flight Mechanics Conference*, Portland, OR, USA, August 2011.
- [7] S.-Y. Oh, S.-C. Kim, D.-K. Lee, S. Kim, and S.-K. Ahn, "Magnus and spin-damping measurements of a spinning projectile using design of experiments," *Journal of Spacecraft and Rockets*, vol. 47, no. 6, pp. 974–980, 2010.
- [8] J. Lijin and T. J. S. Jothi, "Aerodynamic characteristics of an ogive-nose spinning projectile," *Sādhanā*, vol. 43, p. 63, 2018.
- [9] M. Costello and J. Sahu, "Using computational fluid dynamic/rigid body dynamic results to generate aerodynamic models for projectile flight simulation," *Proceedings of the Institution*

- of *Mechanical Engineers, Part G: Journal of Aerospace Engineering*, vol. 222, no. 7, pp. 1067–1079, 2008.
- [10] K. Liang, Z. Huang, and J.-M. Zhang, "Optimal design of the aerodynamic parameters for a supersonic two-dimensional guided artillery projectile," *Defence Technology*, vol. 13, no. 3, pp. 206–211, 2017.
 - [11] J. Allen and M. Ghoreyshi, "Forced motions design for aerodynamic identification and modeling of a generic missile configuration," *Aerospace Science and Technology*, vol. 77, pp. 742–754, 2018.
 - [12] G. T. Chapman and D. B. Kirk, "A method for extracting aerodynamic coefficients from free-flight data," *AIAA Journal*, vol. 8, no. 4, pp. 753–758, 1970.
 - [13] Z.-S. Kuo and H.-Y. Huang, "Parameter identification of spin-stabilized projectiles using a modified Newton-raphson minimization technique," *Transactions of the Japan Society for Aeronautical and Space Sciences*, vol. 43, no. 140, pp. 88–95, 2000.
 - [14] M. Abadir, S. Yusuf, A. Pontillo, and M. Lone, "Parameters estimation methodology for the nonlinear rolling motion of finned cylindrical body," *Aerospace Science and Technology*, vol. 84, pp. 782–798, 2019.
 - [15] V. Condaminet, F. Delvare, D. Choï, H. Demailly, C. Grignon, and S. Heddadj, "Identification of aerodynamic coefficients of a projectile and reconstruction of its trajectory from partial flight data," *Computer Assisted Methods in Engineering and Science*, vol. 21, pp. 177–186, 2017.
 - [16] H. Demailly, F. Delvare, C. Grignon, S. Heddadj, and P. Bailly, "Identification of aerodynamic coefficients of a kinetic energy projectile from flight data," *Inverse Problems in Science and Engineering*, vol. 21, no. 1, pp. 63–83, 2013.
 - [17] Q. Zaikang and D. Lyster, *Multi-Spline Technique for the Extraction of Drag coefficients from radar data (English Edition)*, Journal of Beijing Institute of Technology, Beijing, China, 1994.
 - [18] G. Dutta, A. Singhal, A. Kushari, and A. Ghosh, "Estimation of drag coefficient from radar-tracked flight data of a cargo shell," *Defence Science Journal*, vol. 58, no. 3, pp. 377–389, 2008.
 - [19] B. T. Burchett, "Aerodynamic parameter identification for symmetric projectiles: an improved gradient based method," *Aerospace Science and Technology*, vol. 30, no. 1, pp. 119–127, 2013.
 - [20] C. Montalvo and M. Costello, "Estimation of projectile aerodynamic coefficients using coupled CFD/RBD simulation results," in *Proceedings of the AIAA Atmospheric Flight Mechanics Conference*, Toronto, Canada, August 2010.
 - [21] B. Burchett, "Aerodynamic parameter identification for symmetric projectiles: comparing gradient based and evolutionary algorithms," in *Proceedings of the AIAA Atmospheric Flight Mechanics Conference*, Portland, OR, USA, August 2011.
 - [22] W. Yufei, X. Jiacun, G. Shen, and L. Chen, "Review of aircraft aerodynamic force parameters identification based on the intelligent algorithm," in *Proceedings of the 1st International Workshop on Cloud Computing and Information Security*, Shanghai, China, November 2013.
 - [23] W. Xiaopeng, "Aerodynamic parameter identification of flight vehicles based on adaptive genetic algorithm," *Journal of Astronautics*, vol. 24, pp. 303–308, 2003.
 - [24] J. Guan, W. Yi, S. Chang, and X. Li, "Aerodynamic parameter estimation of a symmetric projectile using adaptive chaotic mutation particle swarm optimization," *Mathematical Problems in Engineering*, vol. 2016, pp. 1–8, 2016.
 - [25] Y. Jiang, C. Dong, and Y. Jia, "Application of artificial bee colony algorithms for unsteady aerodynamic parameter estimation," in *Proceedings of the 2013 Sixth International Symposium on Computational Intelligence and Design*, pp. 152–155, IEEE, Hangzhou, China, April 2013.
 - [26] S. Das, S. S. Mullick, and P. N. Suganthan, "Recent advances in differential evolution—An updated survey," *Swarm and Evolutionary Computation*, vol. 27, pp. 1–30, 2016.
 - [27] R. Storn and K. Price, "Differential evolution—a simple and efficient heuristic for global optimization over continuous spaces," *Journal of Global Optimization*, vol. 11, no. 4, pp. 341–359, 1997.
 - [28] R. Storn and K. Price, *Differential Evolution—A Simple and Efficient Adaptive Scheme for Global Optimization over Continuous Spaces*, ICSI, Berkeley, California, USA, 1995.
 - [29] K. V. Price, R. M. Storn, and J. A. Lampinen, *Differential Evolution: A Practical Approach to Global Optimization*, Springer, Berlin; Germany, 2005.
 - [30] R. Storn and K. Price, "Differential evolution homepage, differential evolution homepage," 2018.
 - [31] U. K. Chakraborty, *Advances in Differential Evolution*, Springer-Verlag, Berlin, Germany, 2008.
 - [32] S. Gajawada, "Vinayaka: a semi-supervised projected clustering method using differential evolution," *International Journal of Software Engineering & Applications*, vol. 3, no. 4, pp. 77–85, 2012.
 - [33] P. Wernert, S. Theodoulis, and Y. Morel, "Flight dynamics properties of 155 mm spin-stabilized projectiles analyzed in different body frames," in *Proceedings of the AIAA Atmospheric Flight Mechanics Conference*, Toronto, Canada, August 2010.
 - [34] D. Regodić, A. Jevremović, and D. Jerković, "The prediction of axial aerodynamic coefficient reduction using base bleed," *Aerospace Science and Technology*, vol. 31, pp. 24–29, 2013.
 - [35] D. Karabog and S. O. Kdem, "A Simple and Global Optimization Algorithm for Engineering Problems," in *Differential Evolution Algorithm*, Springer, Berlin; Germany, 2004.